Supplementary Information

Realization of quantum nanomagnets in metal-free porphyrins

Yan Zhao[1†], Kaiyue Jiang[2†], Can Li[1†], Yufeng Liu[1], Gucheng Zhu[1], Dandan Guan[1,3,4], Yaoyi Li[1,3,4], Hao Zheng[1,3,4], Canhua Liu[1,3,4], Jinfeng Jia[1,3,4], Xiaodong Zhuang[2]*, Shiyong Wang[1,3,4]*

[1]*Key Laboratory of Artificial Structures and Quantum Control (Ministry of Education), Shenyang National Laboratory for Materials Science, School of Physics and Astronomy, Shanghai Jiao Tong University, Shanghai 200240, China*

[2]*The meso-Entropy Matter Lab, School of Chemistry and Chemical Engineering, Shanghai Jiao Tong University, Shanghai 200240, China*

[3]*Tsung-Dao Lee Institute, Shanghai Jiao Tong University, Shanghai, 200240, China*

[4]*Shanghai Research Center for Quantum Sciences, Shanghai 201315, China*

[†]*These authors contributed equally to this work.*

**Corresponding Authors: shiyong.wang@sjtu.edu.cn, zhuang@sjtu.edu.cn*

Table of Contents

Methods

1. Experimental section:

1) Synthetic procedure of 5,15-bis(4-bromo-2,6-dimethylphenyl)porphyrin in solution

A solution of dipyrromethane (1.75 g, 12 mmol) and an 2,6-dimethyl-4-bromobenzaldehyde (12 mmol) in $CHCl_3$ (1.2 L) was treated with $BF_3{\cdot}OEt_2$ (1 mL) at room temperature. The flask was shielded from light with aluminum foil, and the solution was stirred under argon for 8 h. 2,3-dicyano-5,6-dichlorobenzoquinone (4.09 g, 18 mmol) was added and the mixture was stirred at room temperature for 0.5 h. The mixture was neutralized with triethylamine (15 mL). The volume of the solvent was reduced to ca. 300 mL under a reduced pressure. The mixture was filtered through a pad of basic alumina (Merck Aluminum oxide 90 active basic). The filtrate was concentrated and the residue was chromatographed on silica gel. The eluate was evaporated and the resulting solid was purified by recrystallization from CH_2Cl_2/hexane to afford the product (25%)[1].

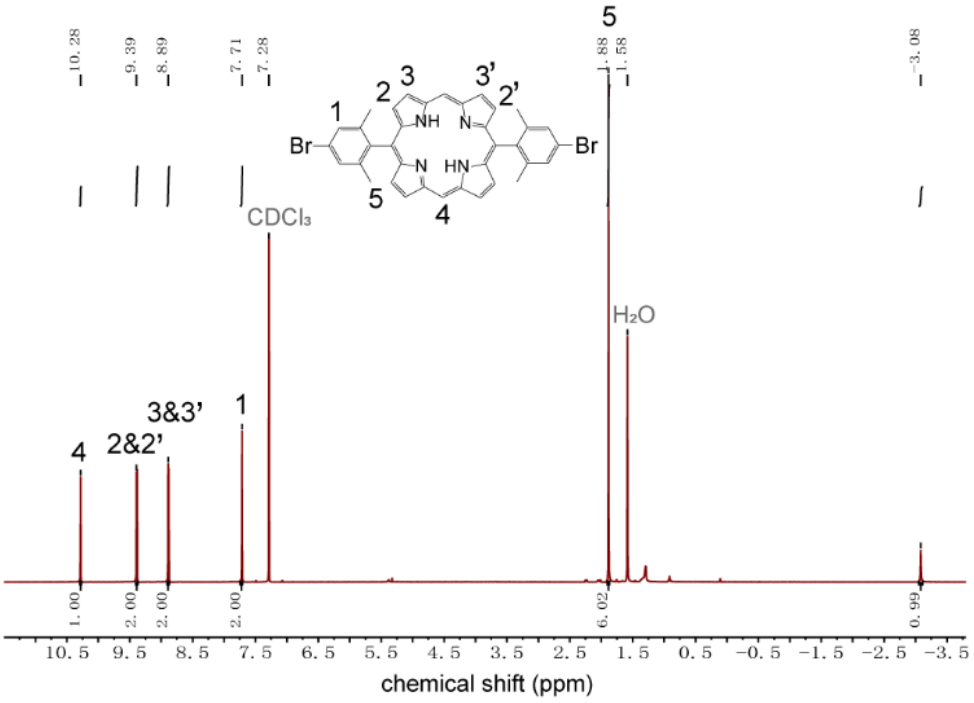

Supplementary Figure 1-1 | ^1H NMR spectrum of 5,15-bis(4-bromo-2,6-dimethylphenyl)porphyrin

2) Synthetic procedure of 5-(2,6-dimethylphenyl)porphyrin precursor in solution

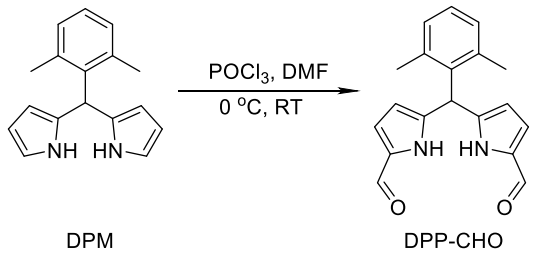

DPM DPP-CHO

To DMF (10 mL) was added $POCl_3$ (1.5 mL, 16.4 mmol) slowly, and the mixture was stirred for 5 min at 0℃. This Vilsmeir reagent (7.5 mL, 10.7 mmol) was added slowly to a solution of 6,5-(2,6-Dimethylphenyl)dipyrromethene (DPM)[2] (1.0 g, 4.5 mmol) in DMF (15 mL), and stirred for 1.5 h at 0℃. The saturated sodium acetate solution (50 mL) was added and stirred at RT overnight. After the reaction completion monitored by TLC, the reaction mixture was diluted with EtOAc, and washed with water and brine. The organic layer was dried over sodium sulfate. The filtrate was concentrated and purified by silica gel column chromatography (DCM : EtOAc = 9 : 1) to give the greenish yellow solid DPP-CHO (860 mg, 70.5%)[3].

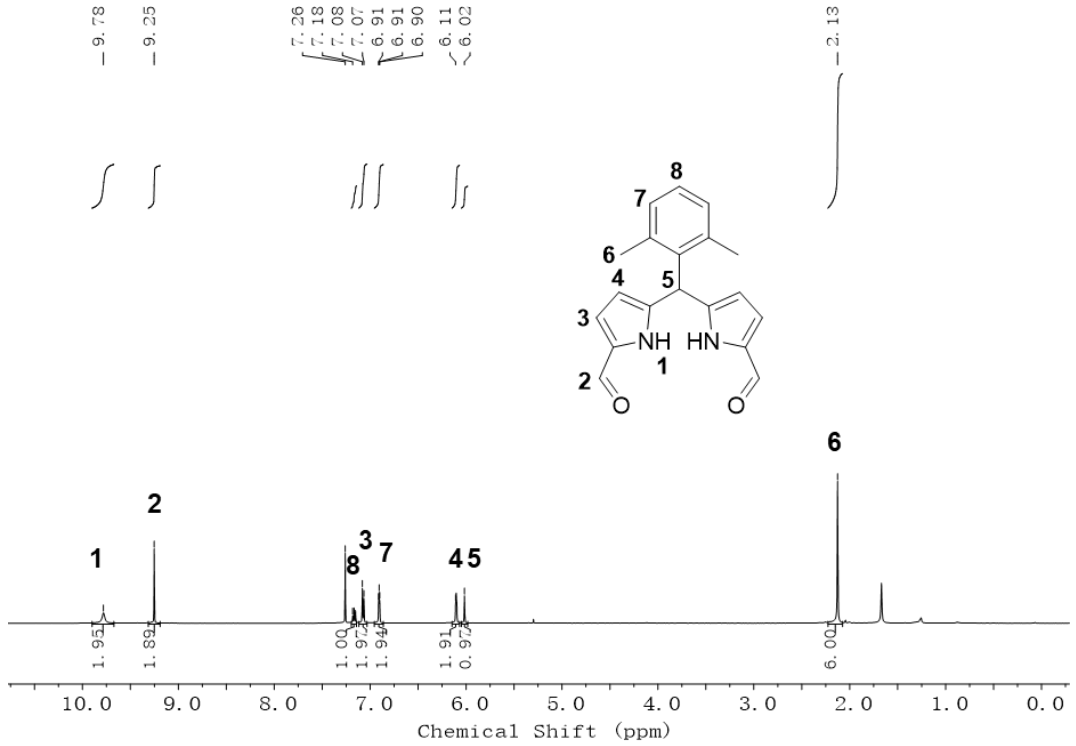

Supplementary Figure 1-2 | ^{1}H NMR spectrum of DPP-CHO.

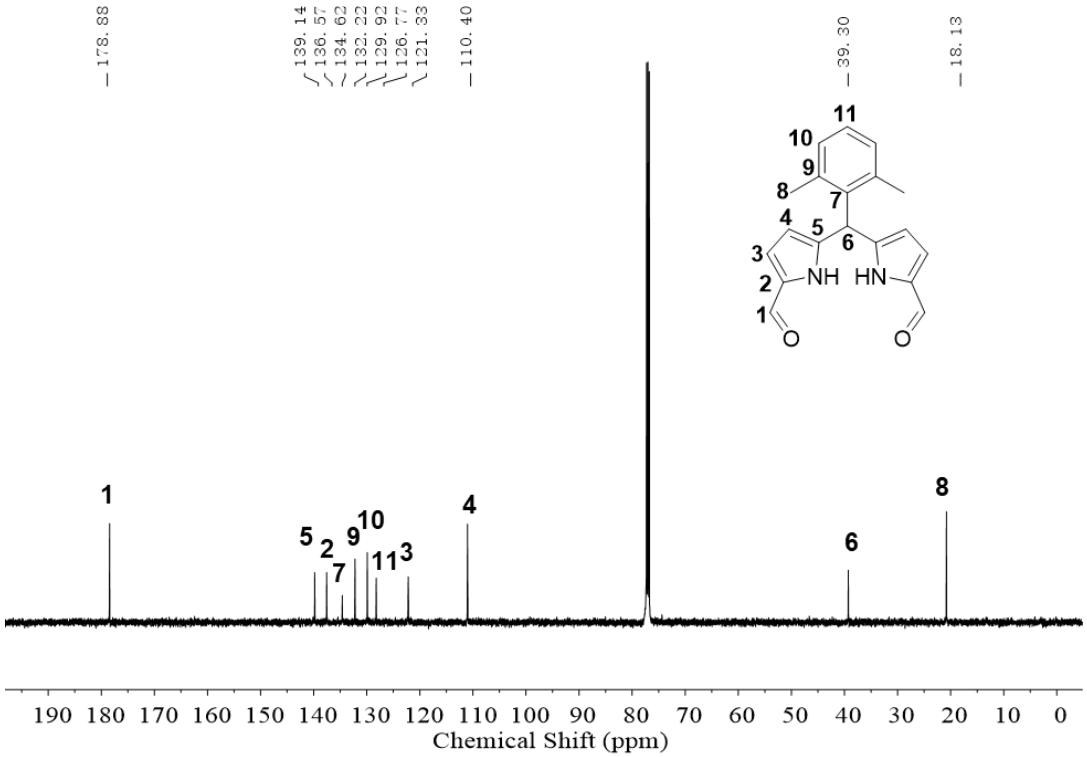

Supplementary Figure 1-3 | ^{13}C NMR spectrum of DPP-CHO.

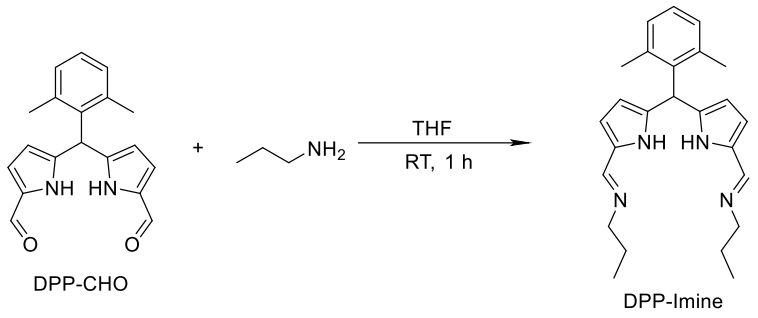

A solution of DPP-CHO (0.300 mmol) and n-propylamine (0.5 mL, 6.08 mmol) in THF (1 mL) was stirred at room temperature for 1 h. Removal of the solvent and excess n-propylamine gave a purple solid DPP-Imine (96%)[3].

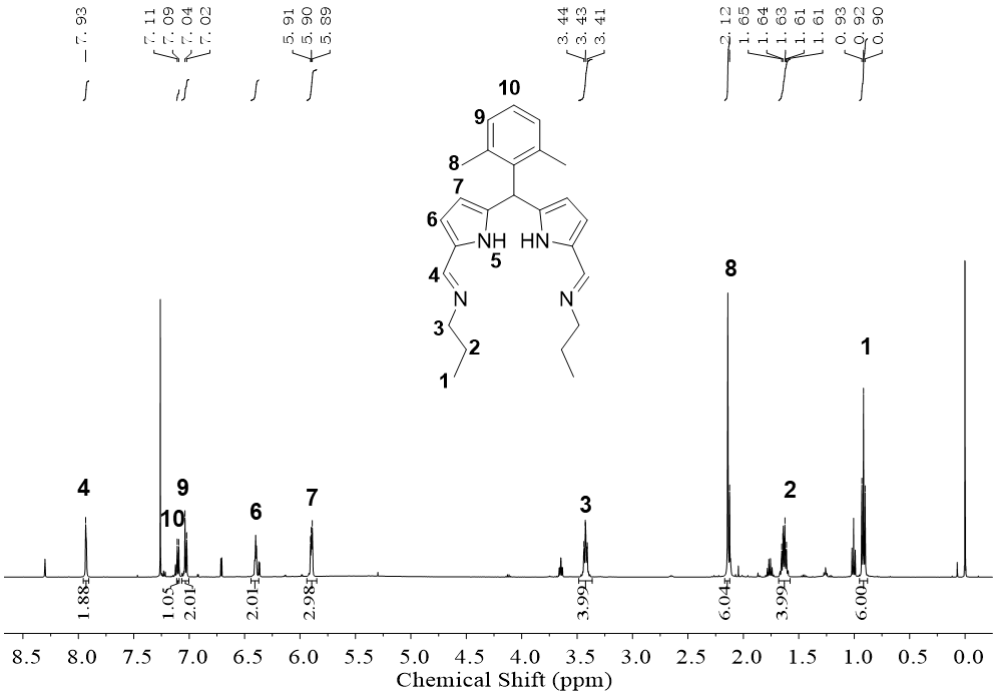

Supplementary Figure 1-4 |^{1}H NMR spectrum of DPP-Imine.

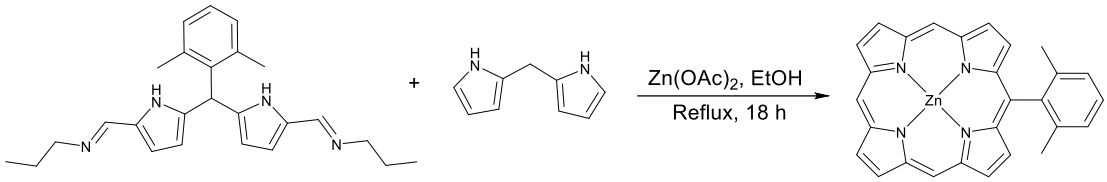

DPP-Imine 3-di-PhMe-Por-Zn

A solution of DPP-Imine [prepared from DPP-CHO (0.300 mmol) in situ] and 5-(p tolyl)dipyrromethane (70.8 mg, 0.300 mmol) in ethanol (30 mL) was treated with $Zn(OAc)_2$ (550 mg, 3.00 mmol) under reflux for 18 h without deaeration. The solvent was removed in vacuo, affording a dark purple residue. The residue was washed with diethyl ether and filtered to remove the excess zinc acetate and pyrrolic polymer byproducts. The filtrate was concentrated to dryness. The residue was washed with diethyl ether and the sparingly soluble polymer byproducts were removed by filtration. The filtrate was concentrated. The procedure was repeated ten times. The resulting crude porphyrin was recrystallized from CH_2Cl_2/cyclohexane affording pure porphyrin 3-di-PhMe-Por (24%).[4] The absence of an added chemical oxidant greatly facilitated purification.

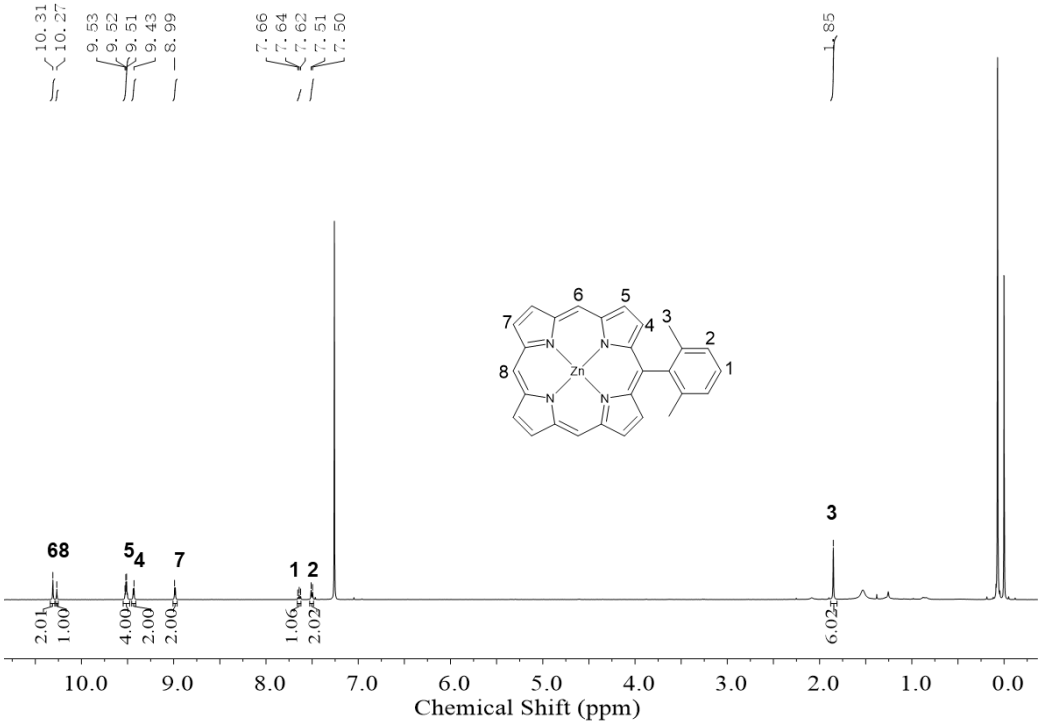

Supplementary Figure 1-5 | ^{1}H NMR spectrum of 1,3-di-PhMe-Por-Zn.

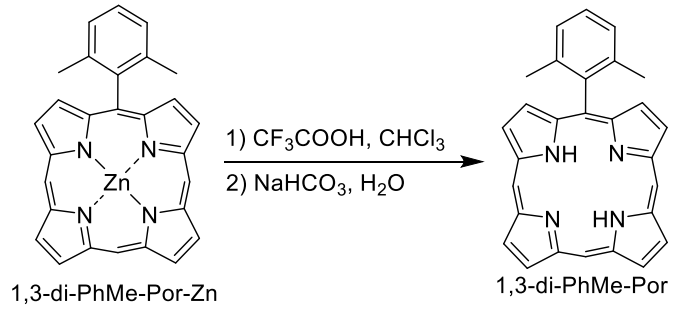

To a stirred solution of 1,3-di-PhMe-Por-Zn (0.405 mmol) in $CHCl_3$ (100 mL) was added trifluoroacetic acid (1.0 mL) at room temperature. After stirring for 12 h, the reaction mixture was neutralized with saturated $NaHCO_3$ aqueous solution (100 mL), and the mixture was extracted with dichloromethane (3 x 100 mL). The combined extracts were dried over anhydrous Na_2SO_4. The solvent was removed under reduced pressure to provide the desired product as a purple red solid (0.390 mmol, 96% yield)[5].

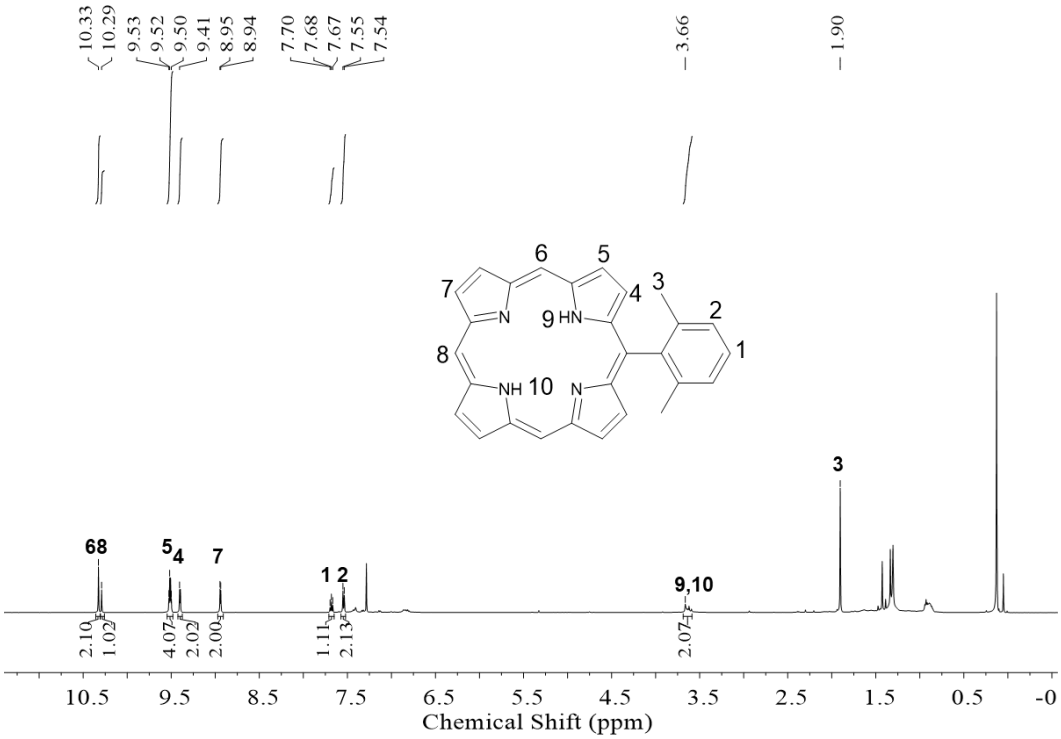

Supplementary Figure 1-6 | ^{1}H NMR spectrum of 5-(2,6-dimethylphenyl)porphyrin

3) Atom manipulation approach

To construct molecular nanomagnets one by one, we performed STM manipulation on the targeted molecular by slowly ramping the bias from 0 to 3V after positioning the STM tip above the sp^3 carbon site and retracting 400pm at the tunneling setpoints of 10mV and 10pA.

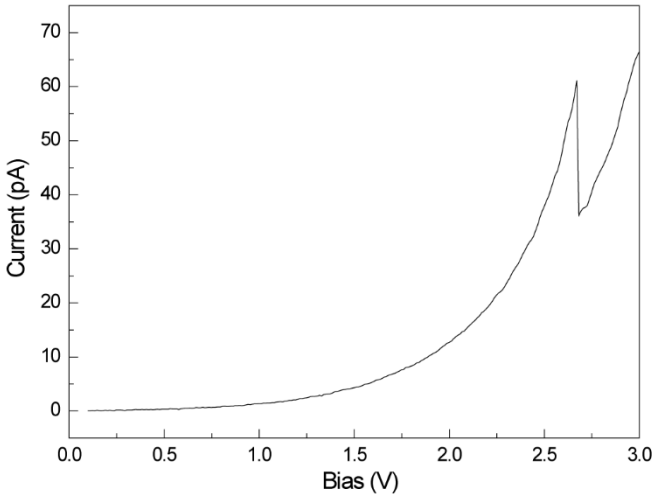

Supplementary Figure 2 | The recorded IV curve during STM manipulation process, with the sudden jump indicating the dissociation of one hydrogen atom.

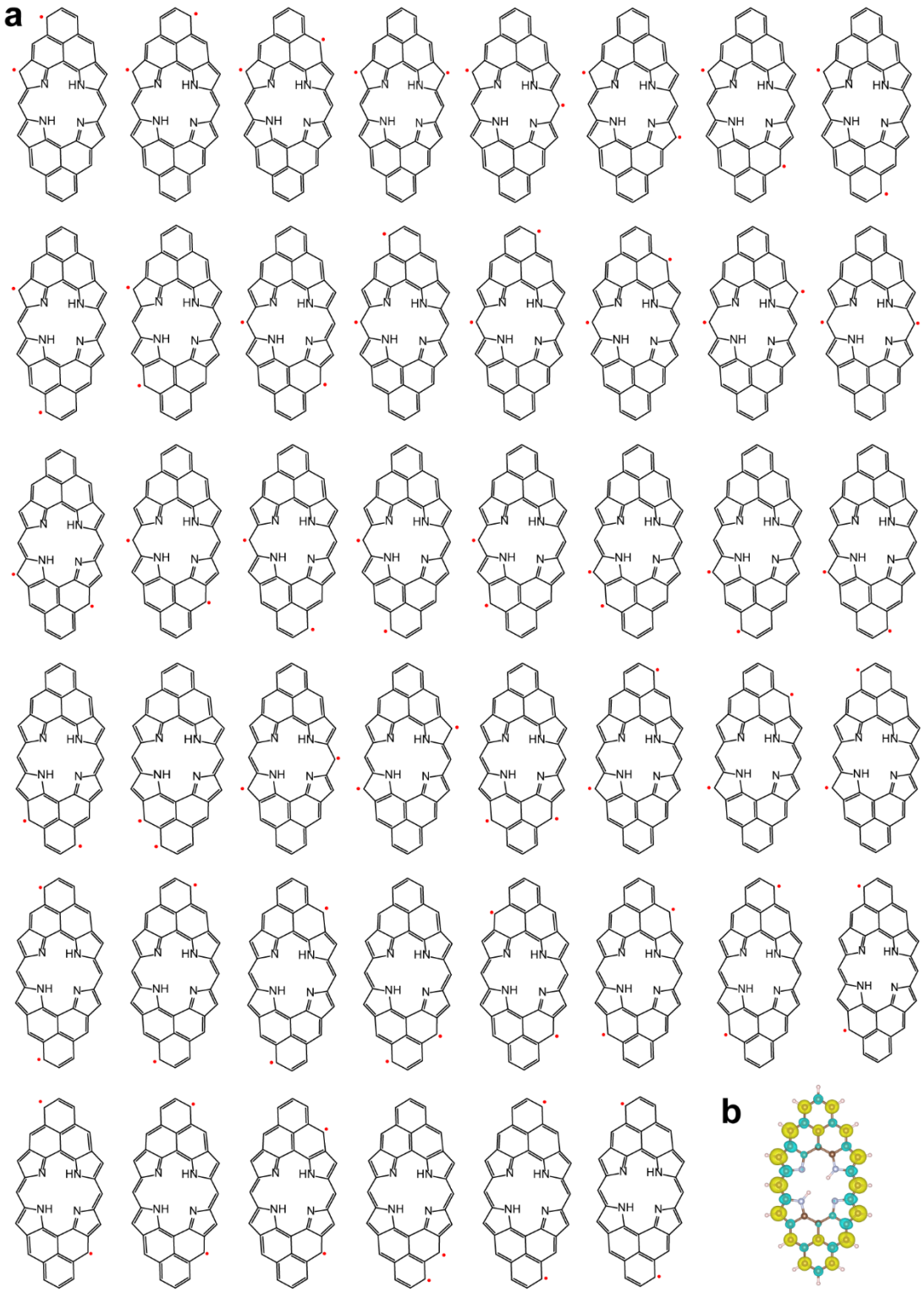

Supplementary Figure 3 | Open shell non-Kekulé resonance structures of the Por monomer. **a,** Open-shell non-Kekulé resonances structures determined by using Clar's empirical rule with the circles indicating Clar's Sextets, red dots indicating the unpaired π-electrons. **b,** Spin-polarized density functional theory calculated spin density distributions. Green: spin up, yellow: spin down. The main features of the calculated spin density distribution maps can be qualitatively related to empirical Clar's non-Kekulé resonance structures [6].

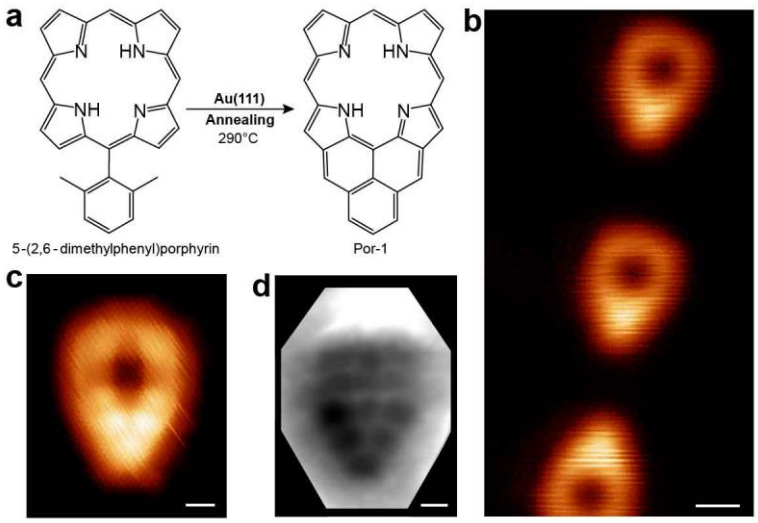

Supplementary Figure 4 | On-surface synthesis of closed-shell porphyrins using the 5-(2,6-dimethylphenyl)porphyrin precursor **a,** Synthetic route. **b**, Constant-height current image of the resulted products on Au(111) (bias voltage: 10 mV, scale bars: 0.5 nm). **c,** High resolution Constant-height current image (bias voltage: 10 mV, scale bars: 0.25 nm). **d,** Nc-AFM frequency shift images (resonant frequency: 28 kHz, oscillation amplitude: 100 pm, Scale bars: 0.2 nm). The resulted products synthesized from the 5-(2,6-dimethylphenyl)porphyrin precursor host a closed-shell electronic structure.

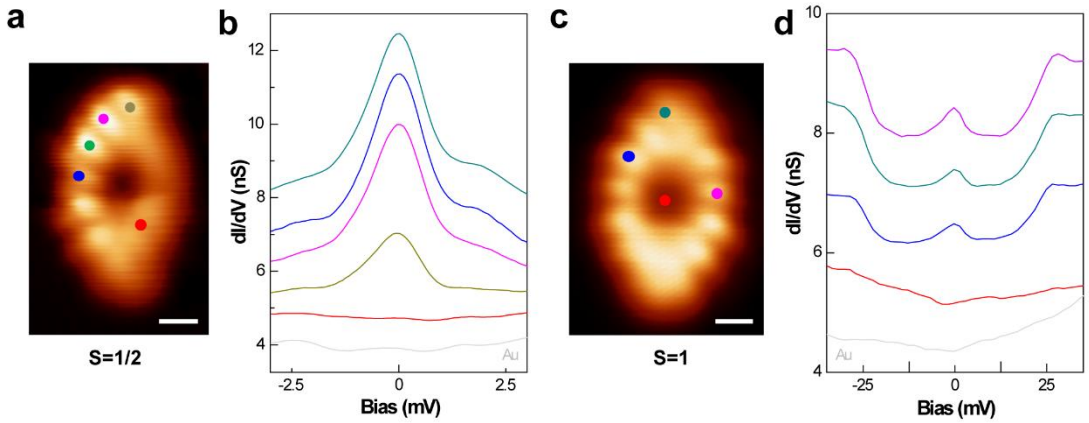

Supplementary Figure 5 | Site-resolved dI/dV spectra of open-shell porphyrin monomers **a,** Constant-height current image (bias voltage: 10 mV, scale bars: 0.28 nm) of the 1H-Por monomer. **b,** D*I*/d*V* spectra taken on the locations marked in **a**. **c,** Constant-height current image (bias voltage: 10 mV, scale bars: 0.26 nm) of the Por monomer. d, D*I*/d*V* spectra taken on the locations marked in **c**.

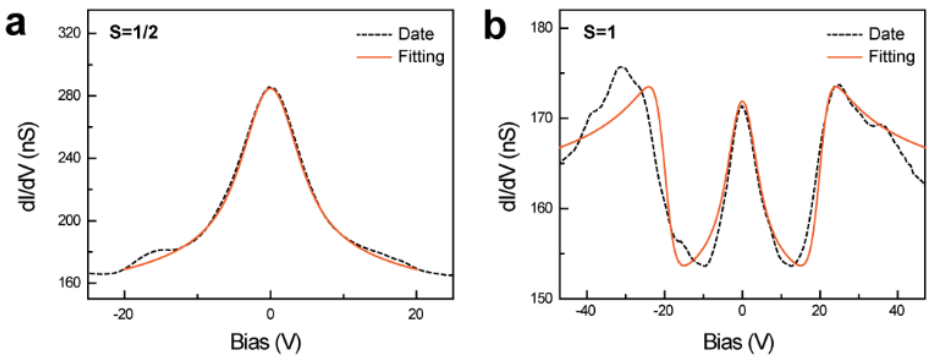

Supplementary Figure 6 | Simulated LDOS spectra of the porphyrin monomers. The LDOS spectra (orange line) are calculated by a perturbation theory to fit the experimental d*I*/d*V* spectra (black lines) of the 1H-Por and Por monomers.

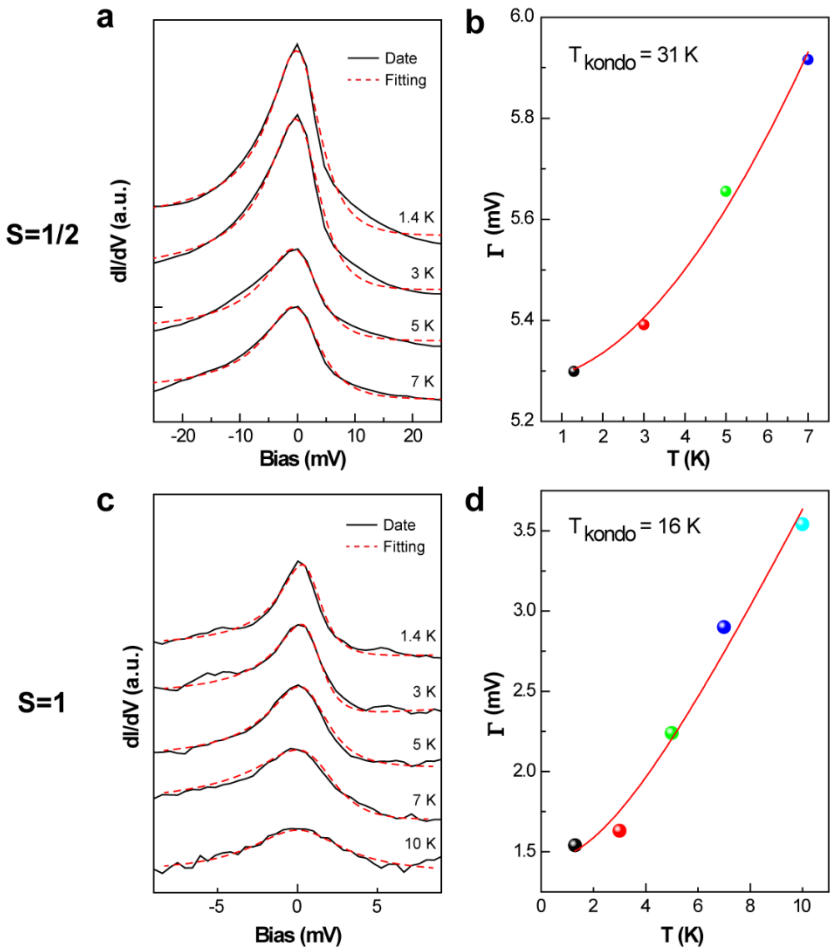

Supplementary Figure 7 | Temperature dependence Kondo resonance spectra **a, c,** Temperature dependence d*I*/d*V* spectra of 1H-Por and Por with dashed lines indicating the fitted curves using a Frota function. **b, d,** The full width at half maximum (FWHM) of Kondo peaks as a function temperature. Solid lines: fitted curves using the equaiton $\Gamma = \sqrt{(\alpha k_B T)^2 + (2k_B T_K)^2}$, where *T* is the temperature, T_K is the Kondo temperature, and α is the slope of linear growth of the width at $T \gg T_K$[7]. A Kondo temperature of 31 K (16K) is obtained for 1H-Por (Por), respectively.

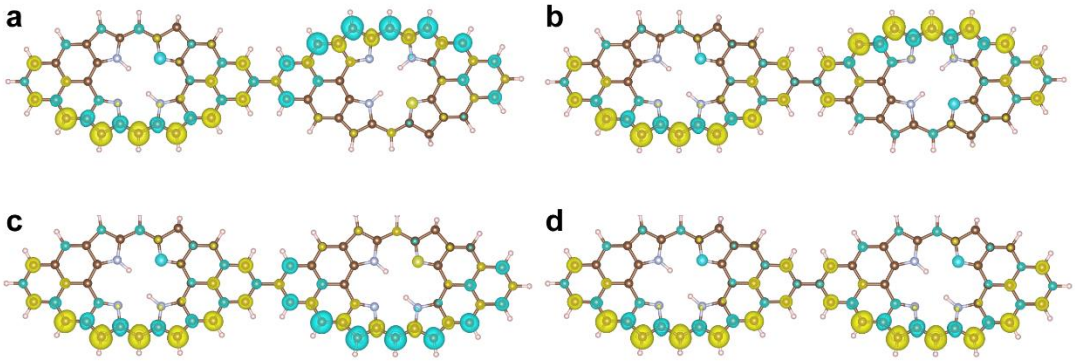

Def2-TZVP	a	b	c	d
Energy (eV)	-87101.5264	-87101.5228	-87101.5332	-87101.5290
Coupling (meV)	-1.8		-2.1	

Supplementary Figure 8 | DFT calculated magnetic coupling strength of Spin S=1/2 dimers. The coupling strength is obtained according to the half of energy difference between ferromagnetic ground state and anti-ferromagnetic ground state.

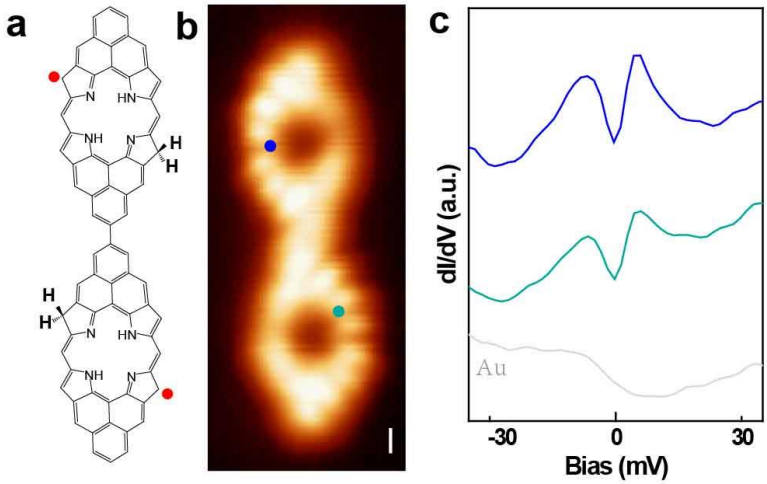

Supplementary Figure 9 | DI/dV spectra showing the magnetic coupling strength of a S=1/2 dimer. **a-b,** Chemical structure and constant-height current image (bias voltage: 10 mV, scale bars: 0.2 nm) of the dimer. **c**, D*I*/d*V* taken on the locations marked in **b**.

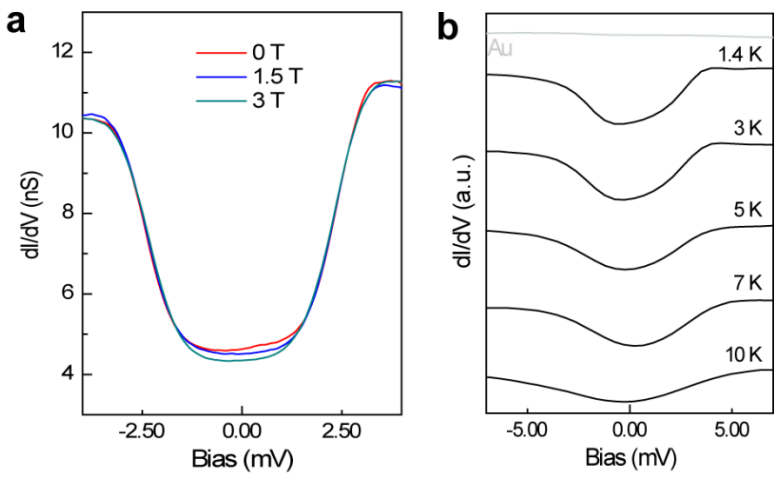

Supplementary Figure 10 | Magnetic field and temperature dependence of the Kondo resonance of porphyrin dimers.

We calculated the finite Heisenberg spin chain using exact diagonalization methods to investigate the excitation features in our dI/dV experiments. The Hamiltonian of Heisenberg model is

$$\hat{H} = -J \sum_{<i,j>} \hat{\vec{S}}_i \cdot \hat{\vec{S}}_j$$

where the J is magnetic coupling strength between two spin $\hat{\vec{S}}_i$ and $\hat{\vec{S}}_j$, which are ferromagnetic coupling for J>0 and anti-ferromagnetic coupling for J<0. The spin $\hat{\vec{S}}_i = \frac{\hbar}{2}\vec{\sigma}_i$ and $\vec{\sigma}_i$ is Pauli matrix for S=1/2. Here, we solved S=1/2 Heisenberg model with spin site number from 2 to 19 under open boundary conditions, which exhibit a rapid decreased excitation gaps in this spin chain.

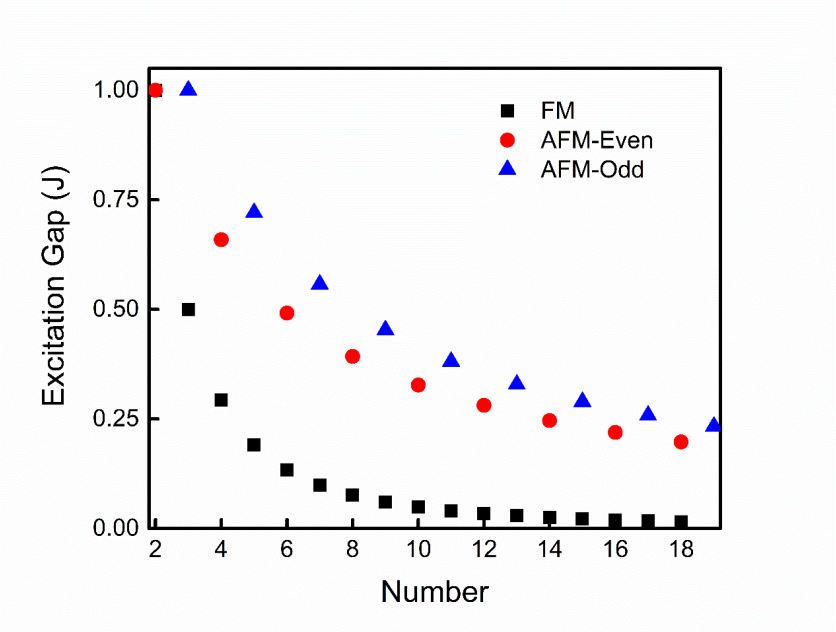

Supplementary Figure 11 | Calculated excitation gap by using isotropic Heisenberg model, with black squares, blue triangles and red circles indicating the lowest excitations of a finite S=1/2 ferromagnetic spin chain, odd-numbered S=1/2 anti-ferromagnetic spin chain and even-numbered S=1/2 anti-ferromagnetic spin chain. The three cases are calculated with open boundary conditions.

To understand the scattering process in STM junction, we fitted our d*I*/d*V* spectra using the perturbation approach up to third order developed by Ternes[8,9]. To reproduce the feature in our d*I*/d*V* spectra data, we set the intramolecular ferromagnetic coupling strength of 20 meV, while the intermolecular magnetic coupling strength of 4 meV (same side) or 3.2 meV (diagonal side). The fitted curves in main Fig. 3-5 are fitted with the parameters of T_{eff}=15 (5) for S=1/2 (S=1) spin chain, and J_{rho}=-0.2. The features are broadened due to finite temperature measurements (T_{eff}) and screening by surface electrons (J_{rho}), as shown in the following two figures.

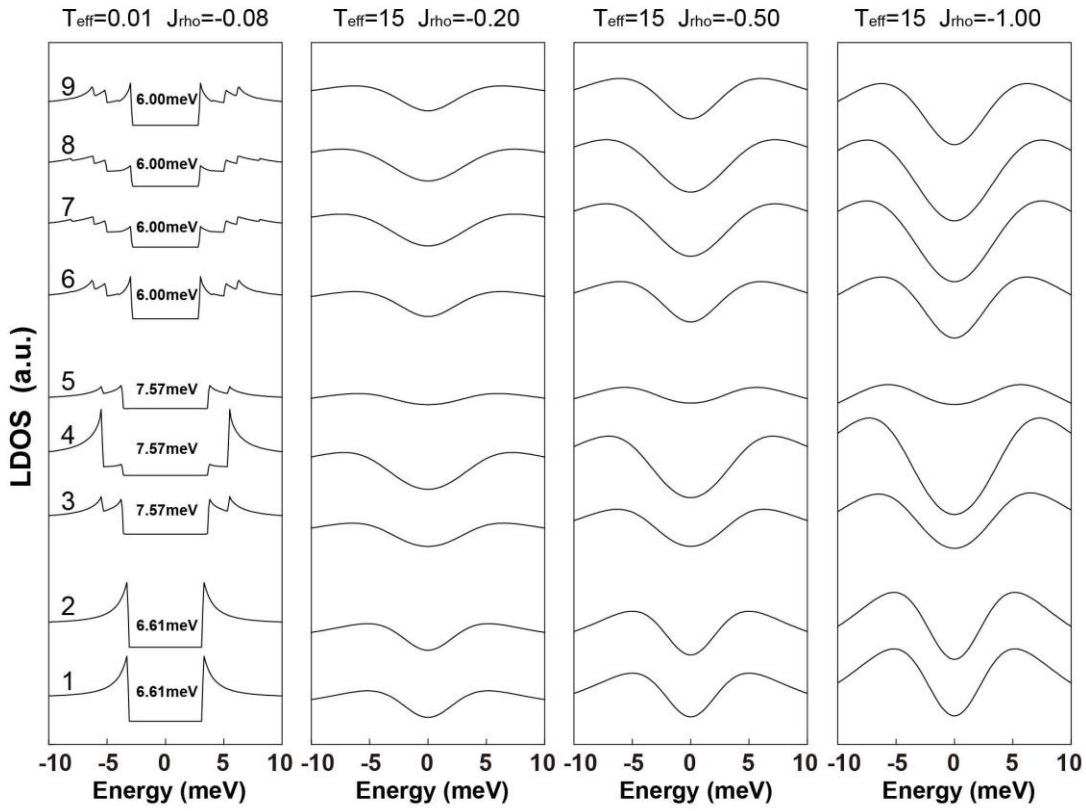

Supplementary Figure 12-1 | Perturbation approach simulated spectra of S=1/2 spin chains.

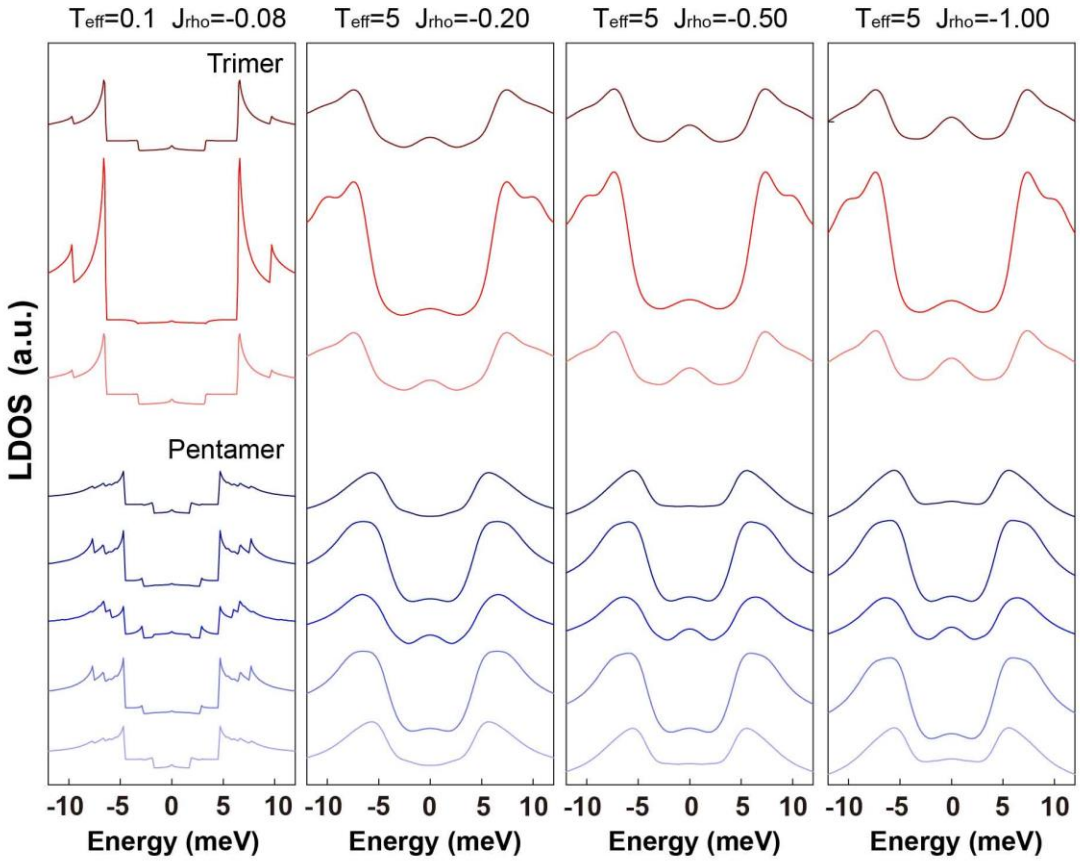

Supplementary Figure 12-2 | Perturbation approach simulated spectra of odd-numbered S=1 spin chains.

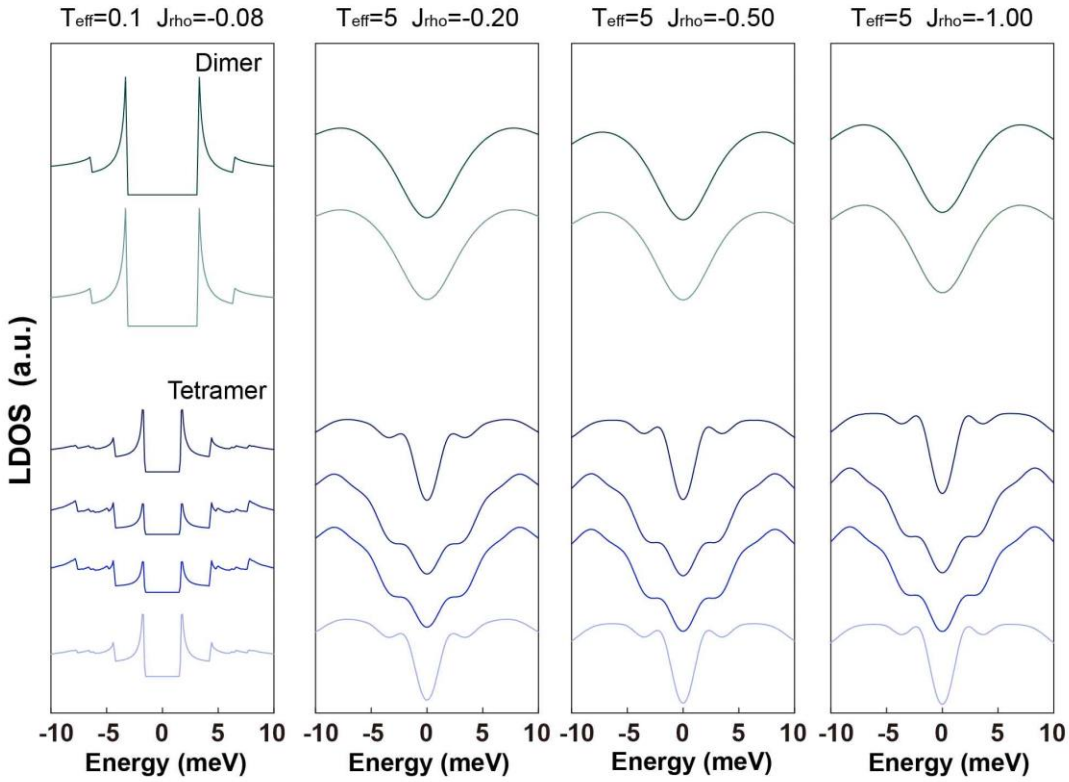

Supplementary Figure 12-3 | Perturbation approach simulated spectra of even-numbered S=1 spin chains.

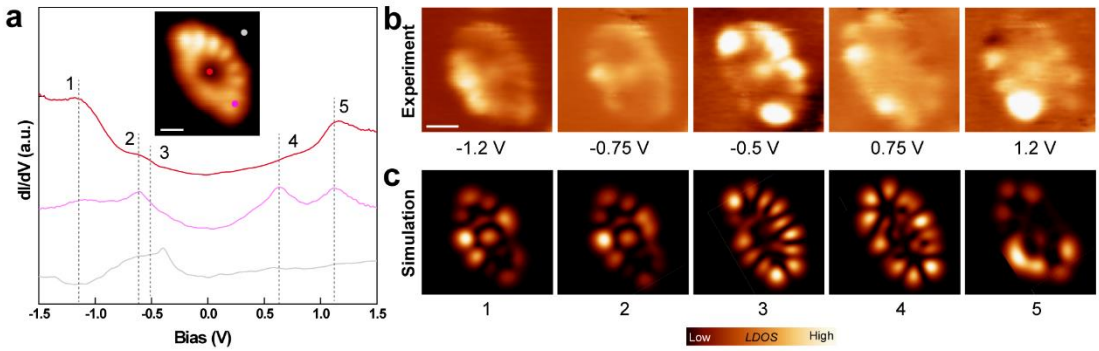

Supplementary Figure 13 | High energy electronic properties of the 1H-Por monomer. **a,** DI/dV spectra taken at the three locations marked on the inset current image (Bias voltage: 10 mV, scare bar: 0.35 nm). **b,** Spatial resolved STS mappings taken at the biases marked in **a**, scare bar: 0.5 nm. **c,** DFT Simulated LDOS mappings.

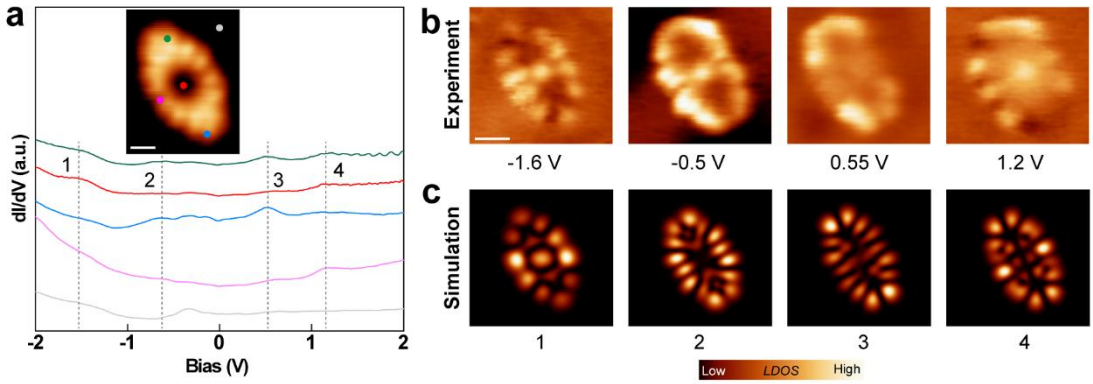

Supplementary Figure 14 | High energy electronic properties of the Por monomer. **a,** DI/dV spectra taken at the five locations marked on the inset current image (Bias voltage: 10 mV, scare bar: 0.35 nm). **b,** Spatial resolved STS mappings taken at the biases marked in **a**, scare bar: 0.5 nm. **c,** DFT Simulated LDOS mappings.

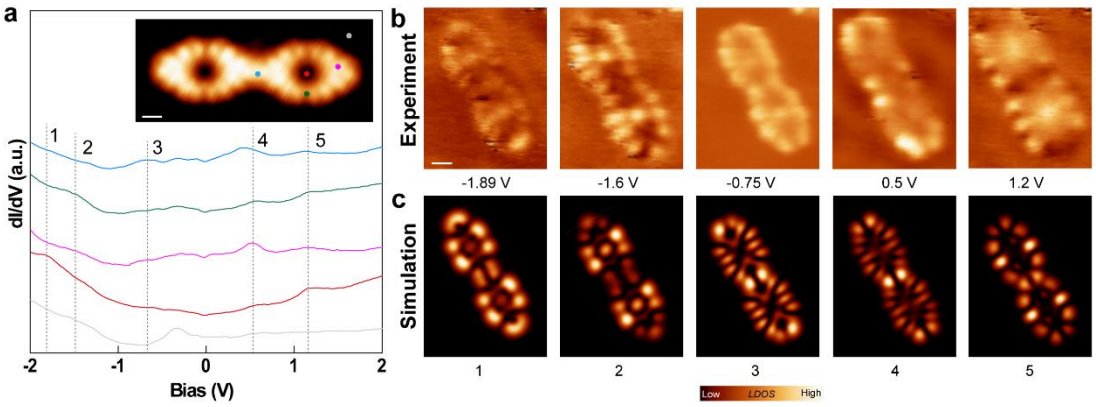

Supplementary Figure 15 | High energy electronic properties of a Por dimer. **a,** DI/dV spectra taken at the five locations marked on the inset current image (Bias voltage: 10 mV, scare bar: 0.35 nm). **b,** Spatial resolved STS mappings taken at the biases marked in **a**, scare bar: 0.5 nm. **c,** DFT Simulated LDOS mappings.

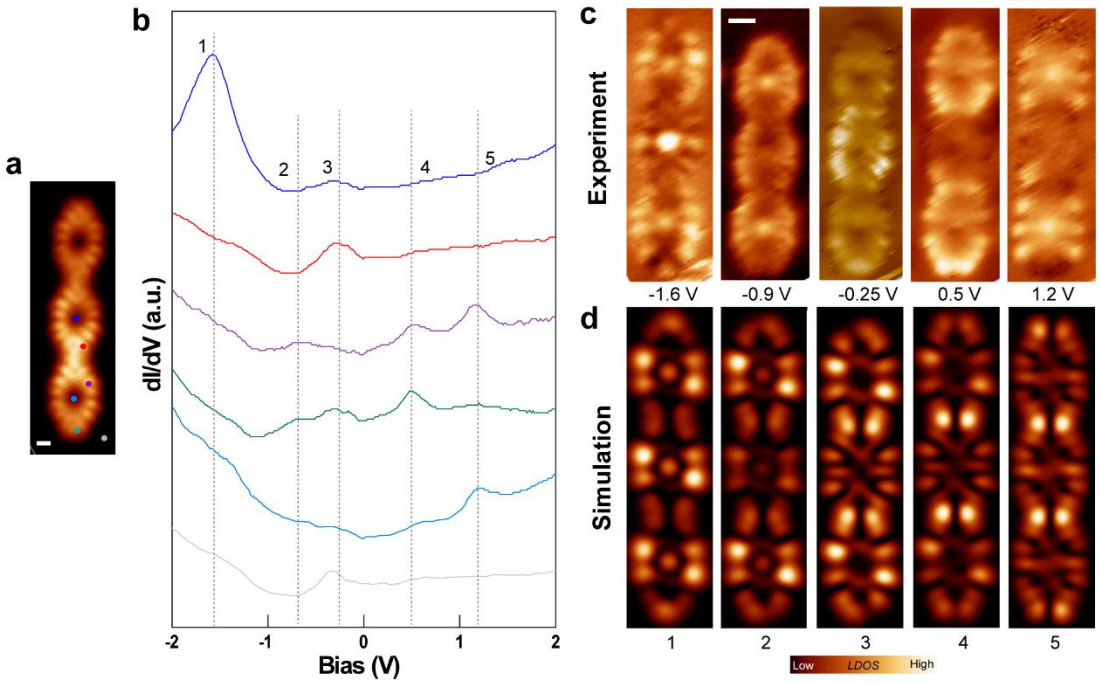

Supplementary Figure 16 | High energy electronic properties of a Por trimer. **a-b,** DI/dV spectra taken at the six locations marked on the left current image (Bias voltage: 10 mV, scare bar: 0.35 nm). **c,** Spatial resolved STS mappings taken at the biases marked in **b**, scare bar: 0.5 nm. **d,** DFT Simulated LDOS mappings.

Reference

1. T. Takanami, A. Wakita, A. Sawaizumi, K. Iso, H. Onodera, K. Suda, Organic Letters 2008, 10, 685-687.
2. P. K. Biswas, S. Saha, Y. Nanaji, A. Rana, M. Schmittel, Inorganic Chemistry 2017, 56, 6662-6670.
3. J.-J. Lee, S.-C. Lee, D. Zhai, Y.-H. Ahn, H. Y. Yeo, Y. L. Tan, Y.-T. Chang, Chem Commun 2011, 47, 4508-4510.
4. M. Taniguchi, A. Balakumar, D. Fan, B. E. McDowell, J. S. Lindsey, Journal of Porphyrins and Phthalocyanines 2005, 09, 554-574.
5. K. Kurotobi, Y. Toude, K. Kawamoto, Y. Fujimori, S. Ito, P. Chabera, V. Sundström, H. Imahori, Chemistry 2013, 19, 17075-17081.
6. Clar, E. Polycyclic Hydrocarbons. (Springer-Verlag Berlin Heidelberg, 1964).
7. Nagaoka, K.; Jamneala, T.; Grobis, M.; Crommie, M. Temperature Dependence of a Single Kondo Impurity. Phys. Rev. Lett. 2002, 88 (7), 077205.
8. Ternes, M. Spin excitations and correlations in scanning tunneling spectroscopy. New J. Phys. 2015, 17, 063016.
9. Ternes, M., Heinrich, A. J. & Schneider, W.-D. Spectroscopic manifestations of the Kondo effect on single adatoms. J. Phys. Condens. Matter. 2009, 21, 053001 (2009).